ACS OMEGA

http://pubs.acs.org/journal/acsodf

Article

Microscale Curling and Alignment of $Ti_3C_2T_x$ MXene by Confining Aerosol Droplets for Planar Micro-Supercapacitors

Yu Wu,[‖] Danjiao Zhao,[‖] Jidi Zhang, Aiping Lin, Yu Wang, Lei Cao, Shufen Wang, Shixian Xiong,* and Feng Gu*

Cite This: *ACS Omega* 2021, 6, 33067−33074

Read Online

ACCESS | Metrics & More | Article Recommendations | Supporting Information

ABSTRACT: Additive manufacturing techniques have revolutionized the field of fabricating micro-supercapacitors (MSCs) with a high degree of pattern and geometry flexibility. However, traditional additive manufacturing processes are based on the functionality of microstructural modulation, which is essential for device performance. Herein, $Ti_3C_2T_x$ MXene was chosen to report a convenient aerosol jet printing (AJP) process for the in situ curling and alignment of MXene nanosheets. The aerosol droplet provides a microscale regime for curling MXene monolayers while their alignment is performed by the as-generated directional stress derived from the quasi-conical fiber array (CFA)-guided parallel droplet flow. Interdigital microelectrodes were further developed with the curled MXene and a satisfying areal capacitance performance has been demonstrated. Importantly, the AJP technique holds promise for revolutionizing additive manufacturing techniques for fabricating future smart microelectronics and devices not only in the microscale but also in the nanoscale.

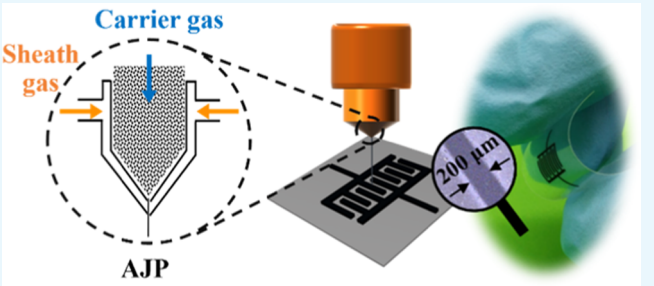

1. INTRODUCTION

With the revolution of portable and wearable electronics, microscale power systems, fabricated at sub-micrometer lengths for on-chip integration, have garnered increasing attention in the last decade.[1−4] However, manufacturing of micro-supercapacitors (MSCs), in particular those that can achieve high energy density with a long lifetime or energy harvesting at a high rate, continually plagues their applications in wearable on-chip microsystems. In comparison with conventional patterning protocols (e.g., lithography, spray masking, and laser scribing), additive manufacturing techniques (e.g., inkjet printing, extrusion printing) offer the potential for scalable production of smart electronics with a high degree of pattern and geometry flexibility by allowing digital and additive patterning, customization, reduction in material waste, scalable and rapid production, and so on.[5−7] However, even with these advantages, challenges still remain that hinder the commercial application of MSCs due to the fact that the filament/ink was simply deposited in a layer-by-layer fashion with the building of the desired three-dimensional (3D) architectures at the microscale while the microstructure, which was essential for electrochemical performance, could not be modulated in situ at the nanoscale.

In comparison, aerosol jet printing (AJP) is seen as another competitive microdevice fabrication technique by virtue of fast-prototyping, wide ink compatibility with minimum printed feature size down to 10 μm.[8−11] Recently, AJP has been developed to create 3D device geometries based on the dynamics of the aerosolized droplets, holding tremendous promise to create complex and intricate geometries with high surface-to-volume ratios for electrodes.[9] Importantly, the aerosolized droplets might serve as droplet-based microreactor systems, showing the potential for the in situ modulation of the microstructures of the printed patterns by virtue of highly controlled, isolated, miniaturized compartmentalization of microscale droplets.[12] Previously, we also synthesized a series of micro/nanostructures (e.g., TiO_2 sphere, ball-in-shell sphere, SnO_2 rod, etc.) by successfully developing aerosol droplets in a flame combustion process.[13,14] Regarding the AJP process, the stream of aerosolized droplets confined in a microscale regime of sheath gas renders the possibilities of creating 3D architectures with controlled microstructures, but these are yet to be reported.

MXenes have come to the fore for a wide range of applications, such as energy storage, electromagnetic interference shielding, and sensors due to highly tunable metallic compositions and surface functional groups.[15−17] Until now, MXene-derived MSCs have been intensively studied via various additive manufacturing processes.[18−21] However, the

Received: September 28, 2021
Accepted: November 10, 2021
Published: November 22, 2021

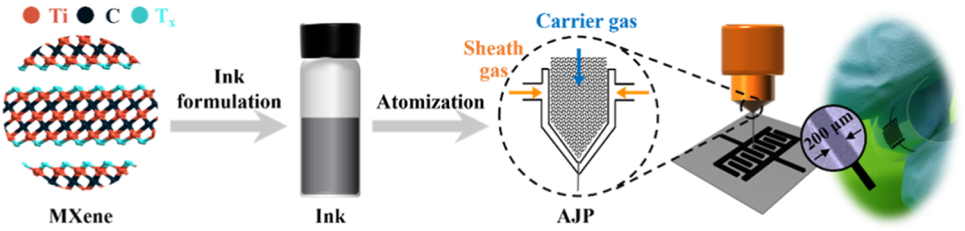

Figure 1. Schematic illustration of the AJP process for MXene patterns.

printed MXene electrode films were mainly composed of densely restacked MXene nanosheets via van der Waals interaction while porous MXene architecture favored an improved electrochemical performance with an enhanced specific surface.[22−24] In view of this dilemma, an additive manufacturing approach offering the capability of microstructure modulation for all-printed MSCs is in high demand for practical applications.

Herein, we successfully realized the in situ curling and alignment of MXene nanosheets via a convenient AJP process by innovatively exploiting the microreactor functionality of aerosol droplets that offer a microscale regime confining the migration of MXene solute loaded in the droplets. In the presence of flow of quasi-conical fiber array (CFA)-guided parallel droplets during the printing process, MXene curling and alignment were achieved with the receding of the monodirectional small meniscus-shaped liquid/solid/gas three-phase contact line (TCL) with the formation of stacked tubular-like nanostructures and the curling degree of MXene was found to be sensitive to the wetting of aerosol droplets. The tentatively fabricated MSC devices of the printed interdigital microelectrode of curled MXene demonstrated competitive electrochemical performance in comparison with the devices fabricated by other additive manufacturing techniques. This work highlights the great potential of AJP for developing devices with the functionality of structure modulation not only at the microscale but also at the nanoscale and broadens the applications of additive manufacturing techniques.

2. RESULTS AND DISCUSSION

The aerosol jet printing process for $Ti_3C_2T_x$ patterns is schematically demonstrated in Figure 1 and the video for the printing process is given in the Supporting Information. The synthetic process of $Ti_3C_2T_x$ MXene nanosheets followed typical procedures reported previously.[23,24] $Ti_3C_2T_x$ MXene, with single- or few-layer thinness and diameters ranging from several hundred nanometers to micrometers, were collected by the chemical etching of the Ti_3AlC_2 precursor, followed by sonication treatment, which can be further characterized and verified by X-ray diffraction (XRD), transmission electron microscopy (TEM), and atomic force microscopy (AFM) (Figure S1). By dispersing the highly hydrophilic $Ti_3C_2T_x$ nanosheets in deionized water, the MXene ink was formulated with a concentration of 10 mg mL^{-1}. Plasma-treated poly(ethylene terephthalate) (PET) plate was chosen as the substrate in this study. During the printing process, the $Ti_3C_2T_x$ ink was atomized, suspended, defined within a carrier gas and a sheath gas of N_2, and directed at the PET substrate that can then be articulated with respect to the deposition head to achieve spatial patterning (Figure 1). To ensure printing quality, the focus ratio (FR), which is defined as the sheath gas flow rate to the ink flow rate, was precisely mediated to minimize overspray, which significantly affects the spatial resolution.[25] In our case, a well-defined line feature of 200 μm could be generated consecutively with effectively reduced overspray when the FR was set at 1.5, as shown in Figure 1. Even after 90 times of cycling printing, the linewidth still remained unchanged and the thickness increased linearly (Figure S2).

Generally, a densely stacked morphology of MXene would be achieved after a traditional vacuum-assisted filtration process (Figure 2a). After the AJP process, the morphology

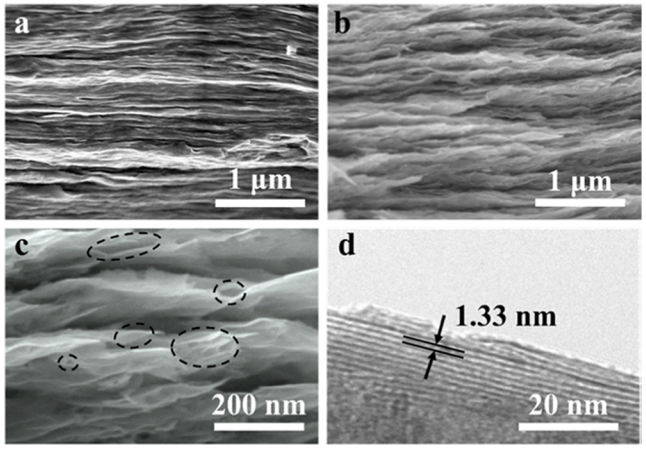

Figure 2. (a) Cross-sectional scanning electron microscopy (SEM) image of restacked $Ti_3C_2T_x$ after vacuum filtration. (b) Cross-sectional SEM image of the printed $Ti_3C_2T_x$ pattern showing a layered architecture. (c) Enlarged SEM image of the pattern showing curled MXene. (d) HRTEM image of the curled MXene.

and microstructure of the MXene pattern changed greatly with the appearance of curled MXene nanosheets forming a tubular-like nanostructure even in the layer-stacked mode (Figure 2b,c). The layered structure originates from the multiple printing passes while the directional alignment follows the nozzle movement. The Brunauer−Emmett−Teller (BET) measurement indicates that the surface area was 25.92 m^2 g^{-1} for the curled $Ti_3C_2T_x$ MXene sample, much higher than that (11.26 m^2 g^{-1}) of the densely stacked $Ti_3C_2T_x$ MXene film via the vacuum-assisted filtration. Generally, electrode architectures with macroporosity are beneficial for increasing the accessibility of electrochemically active sites to ions, especially in the case of decreased pore tortuosity.[23,26,27] The electrode with curled MXene nanosheets is supposed to accommodate more electrochemically active sites for accessing ions while reducing the ion transport lengths greatly. From the high-resolution TEM (HRTEM) image (Figure 2d), we can find that the curled MXene consists of few-layered $Ti_3C_2T_x$ MXene nanosheets rather than a monolayer, indicating that the

https://doi.org/10.1021/acsomega.1c05373
ACS Omega 2021, 6, 33067−33074

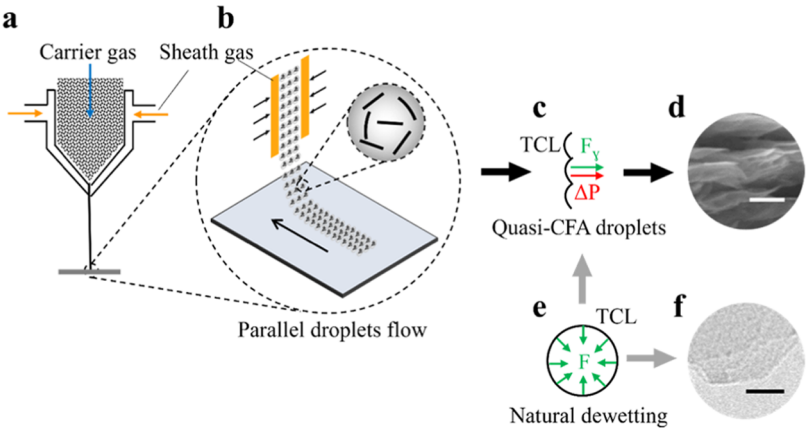

Figure 3. Schematic illustration of the mechanism of MXene curling and alignment during the AJP process. (a) AJP process shows the deposition of the aerosol stream on the substrate surface. (b) Simplified model of generating parallel droplets flow on the surface via the confinement of microscale regime of sheath gas. (c) Multiple monodirectional surface tension derived from small meniscus-shaped TCL dominating the alignment of MXene nanosheets and the curling from the confinement of the microscale regime of droplets. (d–f) Natural dewetting process of a droplet with surface tensions pointing to the normal direction, which results in the formation of flat nanosheets. Scale bar is 100 nm.

reassembly of $Ti_3C_2T_x$ MXene nanosheets occurred during the microreaction process. The interlay distance is estimated to be 1.33 nm, larger than that (1.08 nm) of the previously reported vacuum filtration $Ti_3C_2T_x$ film.[26] In view of the fact that only single-layer $Ti_3C_2T_x$ flakes are present after exfoliation (Figure S1b), the enlarged interlayer distance is expected to further favor the ionic transportation for a promising electrochemical performance. The printed MXene pattern is found to be robust enough and still stable on the PET substrate without falling off or cracking even after being folded 100 times (Figure S3).

The proposed mechanism of MXene curling and alignment during the AJP process is shown in Figure 3. Generally, similar to graphene, the self-restacking and aggregation of MXene nanosheets are usually inevitable during the drying and electrode fabrication processes due to the strong van der Waals interaction between adjacent nanosheets.[26,28] In the case of the AJP process, the $Ti_3C_2T_x$ MXene ink was atomized to form microscale droplets containing MXene nanosheets (Figure 3a). With the deposition of the droplets on the substrate, there exists a temperature gradient along the liquid–vapor interface between the apex and the edge of the droplet, which is indeed the driving force behind the Marangoni flow within drops.[29] Thereby, the MXene nanosheets within the droplet are deemed to be carried by the thermocapillary flows toward the edge and further shaped along the droplet surface. With the evaporation of the solvent (water), the curvature radius (R) of the droplet decreases with the MXene nanosheets migrating outward.[30] Thus, the Laplace pressure, $\Delta P = \frac{2r}{R}$ (r is the surface tension and R is the radius), of the microscale droplet increases greatly along with the deposition on the substrate. It should be noted that MXene is more resistant to bending than graphene due to its larger thickness with high bending rigidity.[16] The curling of MXene nanosheets might be triggered by the sonication that generated the aerosol droplets with stress inequality, and this has been evidenced in previous works on graphene nanoscrolls.[31] The MXene curling would proceed gradually supported by the large ΔP of the microscale droplets. To test this conjecture, we characterized the MXene ink under sonication, the MXene nanosheet was present in the form of a flat structure, and curled MXene nanosheets were hardly identified (Figure 3f). We further collected in situ the aerosol droplets jetted out from the nozzle at 100 °C. Well-defined MXene crumpled nanospheres (~500 nm) were formed via nanosheets curling (Figure S4), identifying the confinement advantage of microscale droplet for nanosheets curling. Recently, Qiu et al. reported an ultrasonication-assisted aerosol spray drying approach for the synthesis of a sphere-like 3D MXene architecture with a loose interior.[32] However, poly(vinylpyrrolidone) (PVP) was used in their work to reduce the surface tension and the aerosol stream was subjected at 600 °C in a tube furnace. In comparison, the curling of MXene occurs without any surfactants in the present work, and the confinement regime of the droplets possibly plays a key role in this structural transformation.

During the AJP process, the depositing droplets stream confined within a sheath gas is considered to form a multiple quasi-parallel directional liquid transfer process, serving as an anchoring point to pin the liquid on the PET substrate or deposited MXene layers while forming microscale slug flow due to the coalescence of droplets (Figure 3b).[33] Basically, a dewetting process is naturally governed by the receding of the TCL and the surface tension F is pointed to the normal direction at certain contacting points (Figure 3e).[34−36] Herein, in the presence of multiple quasi-parallel droplets flowing on the surface, the receding of the TCL is liable to proceed under the multiple quasi-monodirectional surface tension F_γ, as a result of forming numerous small meniscus-shaped TCL curves between each neighboring directional droplets flow (Figure 3c), similar to the conical fibers array (CFA) process reported previously for the alignment of Ag nanowires and a highly oriented polymer film.[36] The $\Delta P = r\left(\frac{1}{R_1} + \frac{1}{R_2}\right)$ (R_1 and R_2 are orthogonal radii of curvature of the small meniscus in this case) of this quasi-CFA-guided parallel droplets flow is helpful for the alignment of MXene nanosheets.[37] Herein, numerous small meniscus-shaped TCL curves are advantageous for giving both a directional stress F_γ with quasi-parallel direction and a large ΔP in the same direction (Figure 3c). The directional stress F_γ forces the MXene to be aligned at the edge of the TCL. Once the free end touched another part of the curled nanosheets due to perturbations, the van der Waals interaction of the overlapped parts decreased the total free energy of MXene, even though the curvature energy increased. In this

https://doi.org/10.1021/acsomega.1c05373
ACS Omega 2021, 6, 33067−33074

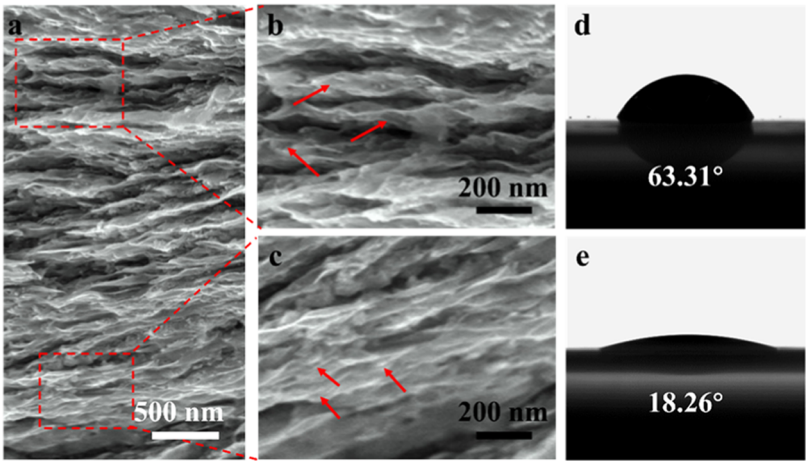

Figure 4. (a) Cross-sectional SEM image of the printed MXene pattern. (b, c) Enlarged SEM image in the top and bottom portions of (a). (d, e) Water droplets on the printed MXene pattern (five printing passes) and the PET substrate.

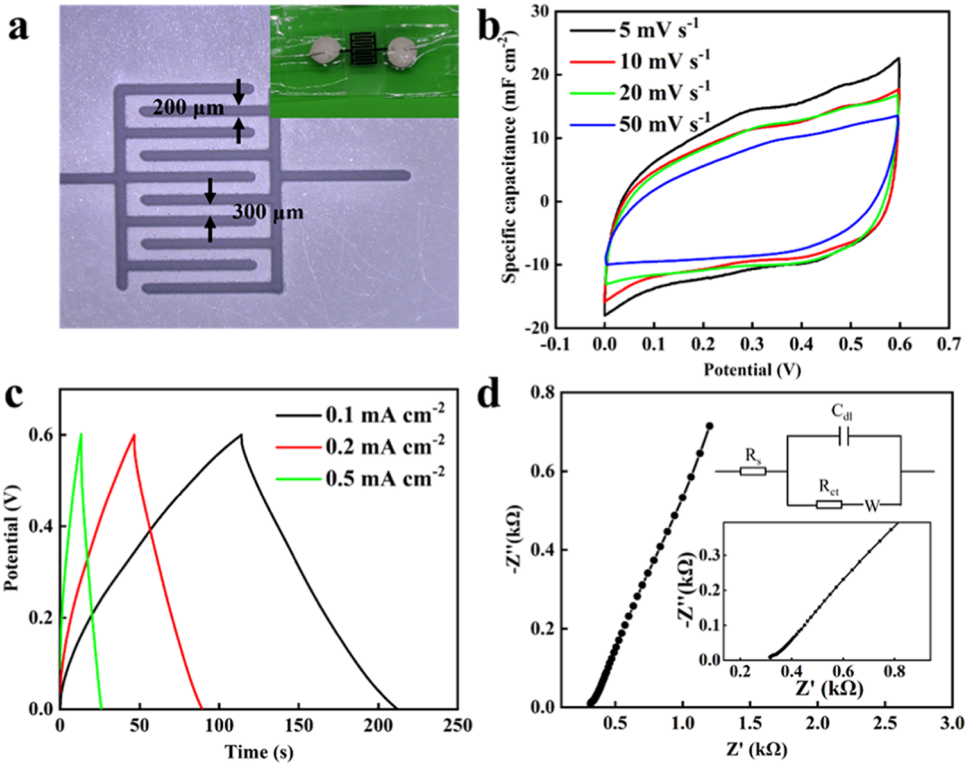

Figure 5. (a) Digital image of the printed interdigital microelectrode of curled MXene and the assembled MSC device is given in the inset. (b) CV curves of the assembled MSC device at different scan rates. (c) GCD profiles of the assembled MSC device at different current densities. (d) Electrochemical impedance spectroscopy of the assembled MSC device. Inset shows the correlative equivalent circuit.

case, the tubular-like nanostructures were preserved (Figure 3d). Previously, several methods have been developed for rolling up graphene, MoS_2, and BN into nanoscrolls by microexplosion, plasma, arc discharge, and high-energy ball milling methods.[38−40] $Ti_3C_2T_x$ MXene scrolls have also been prepared recently by a free drying method with poor morphologies and scrolling from undefined MXene layers.[41] In comparison, the tubular-like $Ti_3C_2T_x$ nanostructure herein was achieved by curling $Ti_3C_2T_x$ nanosheets in situ during the AJP process, showing the potential of facilitating the fabrication of MXene-based devices for future applications.

In addition, the curling degree of $Ti_3C_2T_x$ MXene nanosheets in different portions of the printed patterns is different. The plasma-treated PET substrate showed good hydrophilicity with a contact angle of 18.26° (Figure 4e). With the confinement of hydrophilic substrate, $Ti_3C_2T_x$ MXene nanosheets in the bottom portion tend to deposit with low curvature on the substrate, forming a quasi-planar structure (Figure 4c). With the sequential deposition, the contact angle increases with the formation of curled MXene even if $Ti_3C_2T_x$ MXene is highly hydrophilic to water, making the deposited droplets liable to be pinned. A contact angle of 63.31° was measured for the deposited film after five printing passes (Figure 4d). Accordingly, R at a certain contacting point becomes much smaller as a result of liquid pinning by the number of parallel droplets flow, which renders a better

https://doi.org/10.1021/acsomega.1c05373
ACS Omega 2021, 6, 33067−33074

alignment of tubular-like nanostructures during the printing process (Figure 4b). Meanwhile, the higher curvature of the pinned droplets favors the curling of the nanosheets. As a result, a sharp contrast of curled MXene in the bottom and top portions of the printed patterns was observed (Figure 4a). This observation indicates that the MXene curling and alignment are sensitive to the surface properties of the deposition surface and is worth studying in our future work.

The electrochemical performance of the curled MXene via the AJP process was tentatively investigated by printing interdigital microelectrodes. Considering the excellent electrical conductivity, $Ti_3C_2T_x$ MXene was also employed as a current collector. A well-defined interdigital microelectrode with a linewidth of 200 μm, a thickness of 45 μm, and a gap distance of 300 μm was prepared after 90 printing passes (Figure 5a). The height profile shows the linewidth and thickness for the adjacent electrodes are consistent (Figure S5). The MSC device was fabricated by applying a gel electrolyte based on poly(vinyl alcohol) (PVA)/H_2SO_4 onto the interdigital electrode (inset of Figure 5a). Figure 5b shows the cyclic voltammogram (CV) curves of the MSC device at different scan rates. The quasi-rectangular CV shapes indicate a capacitive charge storage behavior.[42] Galvanostatic charge−discharge (GCD) profiles at different current densities indicate a nearly linear change in the potential during both charge and discharge half-cycles (Figure 5c), revealing an efficient charge storage ability.[43] The slight IR drop in the GCD profile confirms a resistive charge storage behavior, similar to that previously reported for the $Ti_3C_2T_x$ MSC devices.[44] Electrochemical impedance spectroscopy of the assembled MSC device is shown in Figure 5d. The contact resistances between adjacent layers decrease the efficiency of electronic transmission, which generally occurs in the case of a horizontal $Ti_3C_2T_x$ MXene flake alignment with a low out-of-plane electrical conductivity and the dependence of resistance on electrode thickness.[44] On the other hand, the residual terminal groups such as −F and −OH on the $Ti_3C_2T_x$ surface are not conducive to the rapid migration of electrolyte ions between the layers[45] and reduce the number of Ti atoms participating in the redox reaction.[46] The typical areal capacitance of the MSC device was estimated to be 16.33 mF cm^{-2}, while the energy densities were estimated to be 0.817 μWh cm^{-2}, which is apparently higher than that of the MSC device of stacked MXene via a vacuum-assisted filtration process (Figure S6). In addition, we tentatively carried out the cycling tests of the MSC device of curled MXene, which exhibited a satisfying cycling performance with a capacity retention of 90% over 50 cycles (Figure S7). By optimizing the electrode framework (Figure S8), the assembled device exhibited an areal capacitance of 34.87 mF cm^{-2} and an energy density of 1.744 μWh cm^{-2} (Figure S9), exceeding the values of devices fabricated by other additive manufacturing techniques, e.g., direct writing[19] and inkjet printing,[20] reported previously (Supporting Information Table S1). The Coulombic efficiency (CE) was estimated to be 61.4%, which might be attributed to the occurrence of some irreversible parasitic reactions.[47,48] Even in the bending state, the MSC device still exhibited good capacitive behavior and the areal capacitance was estimated to be 28.17 mF cm^{-2} when the bending angle was 90° (Figure S10). The Nyquist plot indicates a pseudocapacitance behavior and the absence of a semicircle shows a good charge transfer behavior (Figure 5d).[49,50] Arising from the specific curled MXene structure, the fabricated microelectrode enables the electrolyte to permeate more readily, enhancing the capacitive performance of this material.[26]

3. CONCLUSIONS

We have demonstrated an interesting AJP approach for the in situ curling and alignment of two-dimensional MXene, which is very challenging for MXene due to its larger thickness with high bending rigidity, for the purpose of developing high-performance portable and wearable electronics. A multiple quasi-parallel directional liquid transfer process developed during the deposition of aerosolized droplets. MXene curling and alignment were achieved simultaneously under the confinement of the microscale regime of droplets and quasi-CFA process offering directional stress and large ΔP in the same direction, resulting in the formation of a layered architecture of curled MXene. To evaluate the electrochemical performance, a planar interdigital microelectrode of curled MXene, which showed a promising areal capacitance of 34.87 mF cm^{-2}, was tentatively developed. Our work further exhibits the potential of the AJP process as a typical additive manufacturing technique for developing future high-performance devices with capabilities of structure modulation at multiscale.

4. EXPERIMENTAL SECTION

4.1. Preparation of Delaminated $Ti_3C_2T_x$. Two grams of lithium fluoride (LiF, Aladdin, China) was added to 40 mL of 9 M hydrogen chloride (HCl, Aladdin, China) and stirred with a magnet for 10 min to clarify at room temperature. Two grams of the Ti_3AlC_2 powder (11 Technology, China) was slowly added to the solution in an ice bath to avoid overheating. Then, the solution was heated to 40 °C and stirred for 48 h. Immediately afterward, the mixture was washed with deionized water and centrifuged and decanted. This procedure was recycled several times until the supernatant pH reached ∼6. After centrifugation, multilayered $Ti_3C_2T_x$ was obtained after freezing the sediment. Then, the multilayered $Ti_3C_2T_x$ was added to a certain amount of deionized water, sonicated for 1 h, and centrifuged for 1 h. Consequently, delaminated $Ti_3C_2T_x$ was obtained after freezing the suspension.

4.2. Preparation of the $Ti_3C_2T_x$ Ink. By simply dispersing 150 mg of delaminated $Ti_3C_2T_x$ in 15 mL of deionized water, the $Ti_3C_2T_x$ ink of 10 mg mL^{-1} was formulated after vigorously shaking and sonicating for 1 h.

4.3. Fabrication of $Ti_3C_2T_x$ Interdigital Electrodes. A commercial AJP printer (WE-HMP, China) was used to print the interdigital electrodes of MXene. The interdigital patterns were designed in the format of .dxf, which can be readable by the printer. The $Ti_3C_2T_x$ ink in a glass vial was atomized in an ultrasonic atomizer (1.7 MHz). The generated aerosol stream was suspended by a carrier gas of N_2 to the print head and jetted out within a sheath gas of N_2 to the plasma-treated PET substrate at ambient temperature. The nozzle diameter was 300 μm and the stand-off height was 5 mm. By precisely mediating the carrier gas flow and sheath gas flow, the overspray could be minimized. In the case of a carrier gas flow of 80 sccm and a sheath gas flow of 120 sccm, a well-defined line feature of 200 μm could be printed. For better studying the influence of the electrode architecture on the device performance, the printed area for all interdigital electrodes was consistent. The printing speed was fixed at 10 mm s^{-1}. The

https://doi.org/10.1021/acsomega.1c05373
ACS Omega 2021, 6, 33067−33074

electrode thickness can be tuned by applying the cycling printing process for each device. The linewidth and gap distance of the electrode could be tuned by designing and introducing variable interdigital patterns into the system.

4.4. Fabrication of $Ti_3C_2T_x$ MSCs. The poly(vinyl alcohol) (PVA)/H_2SO_4 electrolyte was prepared as follows.[49] Five grams of PVA with 87−89% alcohol solubility was added to 25 mL of deionized water and the mixture was stirred in an oil bath at 60 °C for 15 min. Then, 25 mL of deionized water was added to the mixture, followed by stirring at 85 °C for 3 h to obtain a completely transparent solution. The obtained mixture was cooled for 30 min to room temperature. Then, 5 mL of sulfuric acid (98%) was added dropwise and stirred at low speed for 1 h to obtain an electrolyte. The MSC devices were fabricated by applying the obtained gel electrolyte onto the interdigital electrodes with natural drying. Silver wires were connected to the MSCs with the aid of a silver conductive enamel.

4.5. Material Characterizations. X-ray diffraction pattern was obtained with a powder diffractometer (PIGAKV Ultima IV, Japan) using Cu Kα radiation. Scanning electron microscopy (Zeiss Gemini 300, Germany) and transmission electron microscopy (Titan G260-300) were used to acquire the surface morphology images of $Ti_3C_2T_x$ nanosheets. Atomic force microscopy (Bruker Dimension ICON) for measuring the thickness of $Ti_3C_2T_x$ nanosheets. Brunner−Emmet−Teller was used for evaluating the specific surface area (Gold APP V-Sorb 2800P, China). The optical image and the height measurement of the printed patterns were achieved with an optical microscope (Leica DM6 M, Germany).

4.6. Electrochemical Measurement. All electrochemical characterizations were done by an electrochemical workstation (Princeton VersaSTAT 4). According to the common calculation method, the areal capacitance and the energy density of MSCs were calculated from the GCD curves according

$$C_A = \frac{I_t}{S\Delta V} \quad (1)$$

$$E = \frac{1}{2} C_A \Delta V^2 \quad (2)$$

Here, C_A (mF cm^{-2}) is the areal capacitance, I (A) is the discharge current, t (s) is the discharge time, S (cm^2) is the geometric area of the $Ti_3C_2T_x$ electrode, ΔV (V) is the working potential window, and E is the energy density (μWh cm^{-2}).

■ ASSOCIATED CONTENT

Supporting Information

The Supporting Information is available free of charge at https://pubs.acs.org/doi/10.1021/acsomega.1c05373.

Video illustration of the AJP process (MP4)

Schematic illustration of the mechanism of MXene curling and alignment during the AJP process (MP4)

General characterization methods; the dependence of pattern thickness on printing passes; photographs of the printed patterns on PET substrate; the height profile of adjacent patterns; general electrochemical performance characterization; and areal capacitance data of various MSCs (PDF)

■ AUTHOR INFORMATION

Corresponding Authors

Shixian Xiong − *Jiangxi University of Science and Technology, Ganzhou 341000, China; Laboratory of Advanced Materials & Manufacturing (LAMM), Jiangxi Provincial Key Laboratory for Simulation and Modelling of Particulate Systems, Jiangxi University of Science and Technology, Nanchang 330013, China*; Email: s.xiong@jxust.edu.cn

Feng Gu − *Jiangxi University of Science and Technology, Ganzhou 341000, China; Laboratory of Advanced Materials & Manufacturing (LAMM), Jiangxi Provincial Key Laboratory for Simulation and Modelling of Particulate Systems, Jiangxi University of Science and Technology, Nanchang 330013, China; Institute for Process Modelling and Optimization, Jiangsu Industrial Technology Research Institute, Suzhou 215123, China*; Email: feng.gu@jxust.edu.cn

Authors

Yu Wu − *Jiangxi University of Science and Technology, Ganzhou 341000, China; Laboratory of Advanced Materials & Manufacturing (LAMM), Jiangxi Provincial Key Laboratory for Simulation and Modelling of Particulate Systems, Jiangxi University of Science and Technology, Nanchang 330013, China*; orcid.org/0000-0003-2422-057X

Danjiao Zhao − *Jiangxi University of Science and Technology, Ganzhou 341000, China; Laboratory of Advanced Materials & Manufacturing (LAMM), Jiangxi Provincial Key Laboratory for Simulation and Modelling of Particulate Systems, Jiangxi University of Science and Technology, Nanchang 330013, China*

Jidi Zhang − *Institute for Process Modelling and Optimization, Jiangsu Industrial Technology Research Institute, Suzhou 215123, China*

Aiping Lin − *Jiangxi University of Science and Technology, Ganzhou 341000, China; Laboratory of Advanced Materials & Manufacturing (LAMM), Jiangxi Provincial Key Laboratory for Simulation and Modelling of Particulate Systems, Jiangxi University of Science and Technology, Nanchang 330013, China*

Yu Wang − *Jiangxi University of Science and Technology, Ganzhou 341000, China; Laboratory of Advanced Materials & Manufacturing (LAMM), Jiangxi Provincial Key Laboratory for Simulation and Modelling of Particulate Systems, Jiangxi University of Science and Technology, Nanchang 330013, China*

Lei Cao − *Jiangxi University of Science and Technology, Ganzhou 341000, China; Laboratory of Advanced Materials & Manufacturing (LAMM), Jiangxi Provincial Key Laboratory for Simulation and Modelling of Particulate Systems, Jiangxi University of Science and Technology, Nanchang 330013, China*

Shufen Wang − *Jiangxi University of Science and Technology, Ganzhou 341000, China; Laboratory of Advanced Materials & Manufacturing (LAMM), Jiangxi Provincial Key Laboratory for Simulation and Modelling of Particulate Systems, Jiangxi University of Science and Technology, Nanchang 330013, China*

Complete contact information is available at: https://pubs.acs.org/10.1021/acsomega.1c05373

https://doi.org/10.1021/acsomega.1c05373
ACS Omega 2021, 6, 33067−33074

Author Contributions

[‖]Y.W. and D.Z. contributed equally to this work. The manuscript was written through contributions of all authors. All authors have given approval to the final version of the manuscript.

Notes

The authors declare no competing financial interest.

■ ACKNOWLEDGMENTS

This work was financially supported by the Jiangsu Key R&D Plan (BE2018006-4), the JITRI Youth Fellow (GC-1), Suzhou Science and Technology Development Plan (CYTS2019160), the Key Project of Natural Science Foundation of Jiangxi Province (20212ACB203004), and the Planning Project of Jiangxi Provincial Technological Innovation Guidance (20202BDH80003).

■ REFERENCES

(1) Huang, P.; Lethien, C.; Pinaud, S.; Brousse, K.; Laloo, R.; Turq, V.; Respaud, M.; Demortiere, A.; Daffos, B.; Taberna, P. L.; Chaudret, B.; Gogotsi, Y.; Simon, P. On-Chip and Freestanding Elastic Carbon Films for Micro-Supercapacitors. *Science* **2016**, *351*, 691−695.

(2) Zheng, S. H.; Wang, H.; Das, P.; Zhang, Y.; Cao, Y. X.; Ma, J. X.; Liu, S. Z.; Wu, Z. S. Multitasking MXene Inks Enable High-Performance Printable Microelectrochemical Energy Storage Devices for All-Flexible Self-Powered Integrated Systems. *Adv. Mater.* **2021**, *33*, No. 2005449.

(3) Zhang, Y.; Ji, T. X.; Hou, S. H.; Zhang, L. F.; Shi, Y. H.; Zhao, J. X.; Xu, X. H. All-Printed Solid-State Substrate-Versatile and High-Performance Micro-Supercapacitors for In Situ Fabricated Transferable and Wearable Energy Storage via Multi-Material 3D Printing. *J. Power Sources* **2018**, *403*, 109−117.

(4) Zhang, P. P.; Li, Y.; Wang, G.; Wang, F. X.; Yang, S.; Zhu, F.; Zhuang, X. D.; Schmidt, O. G.; Feng, X. L. Zn-Ion Hybrid Micro-Supercapacitors with Ultrahigh Areal Energy Density and Long-Term Durability. *Adv. Mater.* **2019**, *31*, No. 1806005.

(5) Zhang, Y. Z.; Wang, Y.; Cheng, T.; Yao, L. Q.; Li, X. C.; Lai, W. Y.; Huang, W. Printed Supercapacitors: Materials, Printing and Applications. *Chem. Soc. Rev.* **2019**, *48*, 3229−3264.

(6) Li, H. P.; Liang, J. J. Recent Development of Printed Micro-Supercapacitors: Printable Materials, Printing Technologies, and Perspectives. *Adv. Mater.* **2020**, *32*, No. 1805864.

(7) Tian, Z.; Tong, X.; Sheng, G.; Shao, Y.; Yu, L.; Tung, V.; Sun, J.; Kaner, R. B.; Liu, Z. Printable magnesium ion quasi-solid-state asymmetric supercapacitors for flexible solar-charging integrated units. *Nat. Commun.* **2019**, *10*, No. 4913.

(8) Pang, Y. K.; Cao, Y. T.; Chu, Y. H.; Liu, M. H.; Snyder, K.; MacKenzie, D.; Cao, C. Y. Additive Manufacturing of Batteries. *Adv. Funct. Mater.* **2020**, *30*, No. 1906244.

(9) Mishra, S.; Kim, Y. S.; Intarasirisawat, J.; Kwon, Y. T.; Lee, Y.; Mahmood, M.; Lim, H. R.; Herbert, R.; Yu, K. J.; Ang, C. S.; Yeo, W. H. Soft, Wireless Periocular Wearable Electronics for Real-Time Detection of Eye Vergence in a Virtual Reality toward Mobile Eye Therapies. *Sci. Adv.* **2020**, *6*, No. eaay1729.

(10) Abdolmaleki, H.; Kidmose, P.; Agarwala, S. Droplet-Based Techniques for Printing of Functional Inks for Flexible Physical Sensors. *Adv. Mater.* **2021**, *33*, No. 2006792.

(11) Mansoor, N. E.; Muramutsa, F.; Shuck, C. E.; Subbaraman, H.; Pandhi, T.; Gogotsi, Y.; Estrada, D. In *Aerosol Jet Printing of Ti_3C_2 MXene Aqueous Ink*, ECS Meeting Abstracts (No. 12, p. 817); IOP Publishing, 2019; p 817.

(12) Agarwala, S.; Goh, G. L.; Le, T. S. D.; An, J. N.; Peh, Z. K.; Yeong, W. Y.; Kim, Y. J. Wearable Bandage-Based Strain Sensor for Home Healthcare: Combining 3D Aerosol Jet Printing and Laser Sintering. *ACS Sens.* **2019**, *4*, 218−226.

(13) Liu, J.; Hu, Y.; Gu, F.; Li, C. Flame Synthesis of Ball-in-Shell Structured TiO_2 Nanospheres. *Ind. Eng. Chem. Res.* **2009**, *48*, 735−739.

(14) Zhao, Y.; Li, C.; Liu, X.; Go, F.; Du, H. L.; Shi, L. Zn-Doped TiO_2 Nanoparticles with High Photocatalytic Activity Synthesized by Hydrogen-Oxygen Diffusion Flame. *App. Catal., B* **2008**, *79*, 208−215.

(15) Hu, M.; Zhang, H.; Hu, T.; Fan, B.; Wang, X.; Li, Z. Emerging 2D MXenes for Supercapacitors: Status, Challenges and Prospects. *Chem. Soc. Rev.* **2020**, *49*, 6666−6693.

(16) Gogotsi, Y.; Huang, Q. MXenes: Two-Dimensional Building Blocks for Future Materials and Devices. *ACS Nano* **2021**, *15*, 5775−5780.

(17) Pang, J. B.; Mendes, R. G.; Bachmatiuk, A.; Zhao, L.; Ta, H. Q.; Gemming, T.; Liu, H.; Liu, Z. F.; Rummeli, M. H. Applications of 2D MXenes in Energy Conversion and Storage Systems. *Chem. Soc. Rev.* **2019**, *48*, 72−133.

(18) Orangi, J.; Hamade, F.; Davis, V. A.; Beidaghi, M. 3D Printing of Additive-Free 2D $Ti_3C_2T_x$ (MXene) Ink for Fabrication of Micro-Supercapacitors with Ultra-High Energy Densities. *ACS Nano* **2020**, *14*, 640−650.

(19) Quain, E.; Mathis, T. S.; Kurra, N.; Maleski, K.; Van Aken, K. L.; Alhabeb, M.; Alshareef, H. N.; Gogotsi, Y. Direct Writing of Additive-Free MXene-in-Water Ink for Electronics and Energy Storage. *Adv. Mater. Technol.* **2019**, *4*, No. 1800256.

(20) Zhang, C. F.; McKeon, L.; Kremer, M. P.; Park, S. H.; Ronan, O.; Seral-Ascaso, A.; Barwich, S.; Coileain, C. O.; McEvoy, N.; Nerl, H. C.; Anasori, B.; Coleman, J. N.; Gogotsi, Y.; Nicolosi, V. Additive-Free MXene Inks and Direct Printing of Micro-Supercapacitors. *Nat. Commun.* **2019**, *10*, No. 1795.

(21) Yu, L.; Fan, Z.; Shao, Y.; Tian, Z.; Sun, J.; Liu, Z. Versatile N-Doped MXene Ink for Printed Electrochemical Energy Storage Application. *Adv. Energy Mater.* **2019**, *9*, No. 1901839.

(22) Xie, X. Q.; Zhao, M. Q.; Anasori, B.; Maleski, K.; Ren, C. E.; Li, J. W.; Byles, B. W.; Pomerantseva, E.; Wang, G. X.; Gogotsi, Y. Porous Heterostructured MXene/Carbon Nanotube Composite Paper with High Volumetric Capacity for Sodium-Based Energy Storage Devices. *Nano Energy* **2016**, *26*, 513−523.

(23) Lukatskaya, M. R.; Kota, S.; Lin, Z.; Zhao, M.-Q.; Shpigel, N.; Levi, M. D.; Halim, J.; Taberna, P.-L.; Barsoum, M.; Simon, P.; Gogotsi, Y. Ultra-High-Rate Pseudocapacitive Energy Storage in Two-Dimensional Transition Metal Carbides. *Nat. Energy* **2017**, *2*, No. 17105.

(24) Xia, M.; Chen, B.; Gu, F.; Zu, L.; Xu, M.; Feng, Y.; Wang, Z.; Zhang, H.; Zhang, C.; Yang, J. $Ti_3C_2T_x$ MXene Nanosheets as a Robust and Conductive Tight on Si Anodes Significantly Enhance Electrochemical Lithium Storage Performance. *ACS Nano* **2020**, *14*, 5111−5120.

(25) Mahajan, A.; Frisbie, C. D.; Francis, L. F. Optimization of Aerosol Jet Printing for High-Resolution, High-Aspect Ratio Silver Lines. *ACS Appl. Mater. Interfaces* **2013**, *5*, 4856−4864.

(26) Gao, X.; Du, X.; Mathis, T. S.; Zhang, M.; Wang, X.; Shui, J.; Gogotsi, Y.; Xu, M. Maximizing Ion Accessibility in MXene-Knotted Carbon Nanotube Composite Electrodes for High-Rate Electrochemical Energy Storage. *Nat. Commun.* **2020**, *11*, No. 6160.

(27) Xia, Y.; Mathis, T. S.; Zhao, M. Q.; Anasori, B.; Dang, A.; Zhou, Z. H.; Cho, H.; Gogotsi, Y.; Yang, S. Thickness-Independent Capacitance of Vertically Aligned Liquid-Crystalline MXenes. *Nature* **2018**, *557*, 409−412.

(28) Fang, Y.-Z.; Hu, R.; Zhu, K.; Ye, K.; Yan, J.; Wang, G.; Cao, D. Aggregation-Resistant 3D $Ti_3C_2T_x$ MXene with Enhanced Kinetics for Potassium Ion Hybrid Capacitors. *Adv. Funct. Mater.* **2020**, *30*, No. 2005663.

(29) Girard, F.; Antoni, M.; Sefiane, K. On the Effect of Marangoni Flow on Evaporation Rates of Heated Water Drops. *Langmuir* **2008**, *24*, 9207−9210.

(30) Ming, T.; Kou, X.; Chen, H.; Wang, T.; Tam, H.-L.; Cheah, K.-W.; Chen, J.-Y.; Wang, J. Ordered Gold Nanostructure Assemblies

https://doi.org/10.1021/acsomega.1c05373
ACS Omega 2021, 6, 33067−33074

Formed by Droplet Evaporation. *Angew. Chem., Int. Ed.* **2008**, *47*, 9685−9690.
(31) Savoskin, M. V.; Mochalin, V. N.; Yaroshenko, A. P.; Lazareva, N. I.; Konstantinova, T. E.; Barsukov, I. V.; Prokofiev, L. G. Carbon Nanoscrolls Produced from Acceptor-Type Graphite Intercalation Compounds. *Carbon* **2007**, *45*, 2797−2800.
(32) Xiu, L.; Wang, Z.; Yu, M.; Wu, X.; Qiu, J. Aggregation-Resistant 3D MXene-Based Architecture as Efficient Bifunctional Electrocatalyst for Overall Water Splitting. *ACS Nano* **2018**, *12*, 8017−8028.
(33) Xiong, J.; Li, S.; Ciou, J.-H.; Chen, J.; Gao, D.; Wang, J.; Lee, P. S. A Tailorable Spray-Assembly Strategy of Silver Nanowires-Bundle Mesh for Transferable High-Performance Transparent Conductor. *Adv. Funct. Mater.* **2021**, *31*, No. 2006120.
(34) Yang, A. J. M.; Fleming, P. D.; Gibbs, J. H. Molecular Theory of Surface Tension. *J. Chem. Phys.* **1976**, *64*, 3732−3747.
(35) Alejandre, J.; Tildesley, D. J.; Chapela, G. A. Molecular Dynamics Simulation of the Orthobaric Densities and Surface Tension of Water. *J. Chem. Phys.* **1995**, *102*, 4574−4583.
(36) Meng, L. L.; Bian, R. X.; Guo, C.; Xu, B. J.; Liu, H.; Jiang, L. Aligning Ag Nanowires by a Facile Bioinspired Directional Liquid Transfer: toward Anisotropic Flexible Conductive Electrodes. *Adv. Mater.* **2018**, *30*, No. 1706938.
(37) Heikenfeld, J.; Zhou, K.; Kreit, E.; Raj, B.; Yang, S.; Sun, B.; Milarcik, A.; Clapp, L.; Schwartz, R. Electrofluidic Displays Using Young-Laplace Transposition of Brilliant Pigment Dispersions. *Nat. Photonics* **2009**, *3*, 292−296.
(38) Zeng, F.; Kuang, Y.; Wang, Y.; Huang, Z.; Fu, C.; Zhou, H. Facile Preparation of High-Quality Graphene Scrolls from Graphite Oxide by a Microexplosion Method. *Adv. Mater.* **2011**, *23*, 4929−4932.
(39) Meng, J.; Wang, G.; Li, X.; Lu, X.; Zhang, J.; Yu, H.; Chen, W.; Du, L.; Liao, M.; Zhao, J.; Chen, P.; Zhu, J.; Bai, X.; Shi, D.; Zhang, G. Rolling Up a Monolayer MoS_2 Sheet. *Small* **2016**, *12*, 3770−3774.
(40) Bai, Y.; Zhang, J.; Wang, Y.; Cao, Z.; An, L.; Zhang, B.; Yu, Y.; Zhang, J.; Wang, C. Ball Milling of Hexagonal Boron Nitride Microflakes in Ammonia Fluoride Solution Gives Fluorinated Nanosheets That Serve as Effective Water-Dispersible Lubricant Additives. *ACS Appl. Nano Mater.* **2019**, *2*, 3187−3195.
(41) Shah, S. A.; Habib, T.; Gao, H.; Gao, P.; Sun, W.; Green, M. J.; Radovic, M. Template-Free 3D Titanium Carbide ($Ti_3C_2T_x$) MXene Particles Crumpled by Capillary Forces. *Chem. Commun.* **2017**, *53*, 400−403.
(42) Das, P.; Shi, X. Y.; Fu, Q.; Wu, Z. S. Substrate-Free and Shapeless Planar Micro-Supercapacitors. *Adv. Funct. Mater.* **2019**, *30*, No. 1908758.
(43) Yang, W. J.; Yang, J.; Byun, J. J.; Moissinac, F. P.; Xu, J. Q.; Haigh, S. J.; Domingos, M.; Bissett, M. A.; Dryfe, R. A. W.; Barg, S. 3D Printing of Freestanding MXene Architectures for Current-Collector-Free Supercapacitors. *Adv. Mater.* **2019**, *31*, No. 1902725.
(44) Zhang, C. F.; Kremer, M. P.; Seral-Ascaso, A.; Park, S. H.; McEvoy, N.; Anasori, B.; Gogotsi, Y.; Nicolosi, V. Stamping of Flexible, Coplanar Micro-Supercapacitors Using MXene Inks. *Adv. Funct. Mater.* **2018**, *28*, No. 1705506.
(45) Tang, Q.; Zhou, Z.; Shen, P. W. Are MXenes Promising Anode Materials for Li Ion Batteries? Computational Studies on Electronic Properties and Li Storage Capability of Ti_3C_2 and $Ti_3C_2X_2$ (X = F, OH) Monolayer. *J. Am. Chem. Soc.* **2012**, *134*, 16909−16916.
(46) Shao, H.; Xu, K.; Wu, Y.-C.; Iadecola, A.; Liu, L.; Ma, H.; Qu, L.; Raymundo-Piñero, E.; Zhu, J.; Lin, Z.; Taberna, P.-L.; Simon, P. Unraveling the Charge Storage Mechanism of $Ti_3C_2T_x$ MXene Electrode in Acidic Electrolyte. *ACS Energy Lett.* **2020**, *5*, 2873−2880.
(47) Navarro-Suárez, A. M.; Van Aken, K. L.; Mathis, T.; Makaryan, T.; Yan, J.; Carretero-Gonzalez, J.; Rojo, T.; Gogotsi, Y. Development of asymmetric supercapacitors with titanium carbide-reduced graphene oxide couples as electrodes. *Electrochim. Acta* **2018**, *259*, 752−761.
(48) Fan, Z. D.; Wei, C. H.; Yu, L. H.; Xia, Z.; Cai, J. S.; Tian, Z. N.; Zou, G. F.; Dou, S. X.; Sun, J. Y. 3D Printing of Porous Nitrogen-Doped Ti_3C_2 MXene Scaffolds for High-Performance Sodium-Ion Hybrid Capacitors. *ACS Nano* **2020**, *14*, 867−876.
(49) Wu, C. W.; Unnikrishnan, B.; Chen, I. W. P.; Harroun, S. G.; Chang, H. T.; Huang, C. C. Excellent Oxidation Resistive MXene Aqueous Ink for Micro-Supercapacitor Application. *Energy Storage Mater.* **2020**, *25*, 563−571.
(50) Abdolhosseinzadeh, S.; Schneider, R.; Verma, A.; Heier, J.; Nuesch, F.; Zhang, C. F. Turning Trash into Treasure: Additive Free MXene Sediment Inks for Screen-Printed Micro-Supercapacitors. *Adv. Mater.* **2020**, *32*, No. 2000716.

https://doi.org/10.1021/acsomega.1c05373
ACS Omega 2021, 6, 33067−33074